Cancer cell CD44 mediates macrophage/monocyte-driven regulation of head and neck cancer stem cells

Karina E. Gomez[1], **FangLong Wu**[2,3], **Stephen B. Keysar**[1], **J. Jason Morton**[1], **Bettina Miller**[1], **Tugs-Saikhan Chimed**[1], **Phuong N. Le**[1], **Cera Nieto**[1], **Farshad N. Chowdhury**[1], **Anit Tyagi**[1], **Traci R. Lyons**[1,4], **Christian D. Young**[2], **Hongmei Zhou**[3], **Hilary L. Somerset**[2], **Xiao-Jing Wang**[2,4,5], **Antonio Jimeno**[1,4]

[1]Division of Medical Oncology, Department of Medicine, University of Colorado Anschutz Medical Campus (CU AMC), CO, 80045.

[2]Department of Pathology, CU AMC, CO, 80045.

[3]State Key Laboratory of Oral Diseases, Department of Oral Medicine, West China Hospital of Stomatology, Sichuan University, Chengdu, China.

[4]Gates Center for Regenerative Medicine, CU AMC, CO, 80045.

[5]Veterans Affairs Medical Center, VA Eastern Colorado Health Care System, Aurora, CO, USA.

Abstract

Tumor-associated macrophages (TAM) in the tumor microenvironment (TME) cooperate with cancer stem cells (CSC) to maintain stemness. We recently identified CD44 as a surface marker defining head and neck squamous cell carcinoma (HNSCC) CSC. PI3K-4EBP1-SOX2 activation and signaling regulate CSC properties, yet the upstream molecular control of this pathway and the mechanisms underlying crosstalk between TAM and CSC in HNSCC remain largely unknown. Because CD44 is a molecular mediator in the TME, we propose here that TAM-influenced CD44 signaling could mediate stemness via the PI3K-4EBP1-SOX2 pathway, possibly by modulating availability of hyaluronic acid (HA), the main CD44 ligand. HNSCC IHC was used to identify TAM/CSC relationships, and in vitro co-culture spheroid models and in vivo mouse models were used to identify the influence of TAM on CSC function via CD44. Patient HNSCC-derived TAM were positively and negatively associated with CSC marker expression at non-invasive and invasive edge regions, respectively. TAM increased availability of HA and increased cancer cell invasion. HA binding to CD44 increased PI3K-4EBP1-SOX2 signaling and the CSC fraction,

whereas CD44-VCAM-1 binding promoted invasive signaling by Ezrin/PI3K. In vivo, targeting CD44 decreased PI3K-4EBP1-SOX2 signaling, tumor growth, and CSC. TAM depletion in syngeneic and humanized mouse models also diminished growth and CSC numbers. Lastly, a CD44 isoform switch regulated epithelial-to-mesenchymal plasticity as CD44s and CD44v8-10 determined invasive and tumorigenic phenotypes, respectively. We have established a mechanistic link between TAM and CSC in HNSCC that is mediated by CD44 intracellular signaling in response to extracellular signals.

Keywords

Head and neck squamous cell cancer; cancer stem cells; CD44; TAMs; macrophage; monocytes; VCAM-1; PI3K; SOX2; stemness; invasion; HAS2; ZEB1; ESRP1

INTRODUCTION

U.S. head and neck squamous cell carcinoma (HNSCC) incidence increased from 35,310 in 2008 to 51,540 in 2018, due to rising human papillomavirus (HPV) positive cases and stable HPV-negative incidence (1–4). Cancer stem cells (CSCs) have pro-tumorigenic abilities including self-renewal, resistance to therapy, and maintenance of tumor heterogeneity (5–7). Recent reports have increased our understanding of HNSCC CSC biology (8,9), and regulation by both intrinsic and extrinsic mechanisms via the tumor microenvironment (TME) (10).

The cluster of differentiation 44 receptor (CD44), a CSC marker conserved across cancer types, drives pro-tumorigenic signaling and regulates CSC 'stemness' (11,12). We identified CD44 (together with Aldefluor activity) as a HNSCC CSC marker (9). Its structure and ligand-binding functions allow CD44 to serve as an extracellular sensor and link between TME cues and intrinsic cancer cell signaling (13). Human *CD44* has 19 exons, 10 of which are constant, or present, in all variants and make up the standard form of CD44 (CD44s). The variants of CD44 (CD44v) are encoded by alternative splicing and consist of the 10 constant exons in any combination with the remaining 9 variant exons (14). CD44 isoforms have both overlapping and unique roles, however all include extracellular matrix (ECM) binding motifs that promote interaction with the microenvironment and facilitate activation of various signaling pathways (14) to grant cancer cells adaptive plasticity in response to microenvironment changes (15). Hyaluronic acid (HA), a major component of the ECM, is expressed by tumor and stromal cells via hyaluronan synthases (HASes) and is the most specific ligand for CD44 activation; the HA binding domain is found on all CD44 isoforms (11).

Tumor-associated macrophages (TAMs) are critical for tumor progression; they promote angiogenesis, immune suppression, metastasis, and chemotherapy resistance, in addition to their influence on CSC stemness (16). Studies in renal, breast, and colon cancers have demonstrated TAM involvement in promoting CD44 expression and signaling (17–19). In addition, several reports demonstrate the ability of TAMs to directly modulate CSCs and expression of their markers (20,21), including regulation of SOX2 (sex determining region Y box 2), a transcription factor strongly associated with stemness (22–24). Although clinical

correlation studies have suggested an association between TAM presence and SOX2 expression in HNSCC (25), the cellular and molecular mechanisms underlying TAM regulation of CSCs remain largely unknown.

We recently reported that phosphoinositide 3 kinase/mammalian target of rapamycin/ eukaryotic translation initiation factor 4E-binding protein (PI3K/mTOR/4EBP1) signaling regulates fundamental CSC genes. Specifically, activated PI3K/mTOR phosphorylates 4EBP1, a step confirmed with PI3K inhibitors, and phosphorylated 4EBP1 promoted release of eIF4E which increased SOX2 translation. SOX2 was found to directly upregulate aldehyde dehydrogenase 1A1 (*ALDH1A1*) transcription, thus regulating and maintaining CSC stemness in HNSCCs (9). However, the upstream regulation of PI3K in relation to downstream SOX2 signaling is not known. Although a complex interplay between TAMs and cancer cells is known to exist in the field of cancer research, we limited our study to the scope of our previously published pathway for feasibility and cohesiveness. Here we sought to build upon this work and determine 1) the upstream involvement of the CD44 receptor in PI3K-4EBP1-SOX2 regulation, and 2) how TAMs modulate stemness using CD44 as a mediator. We identified two distinct relationships between TAMs and tumor cells related to 1) stemness/growth promotion and 2) invasion using HNSCC patient tumor samples. We further verified these relationships using *in vitro* co-culture spheroid systems and *in vivo* models.

We report that the presence of TAMs can promote both stemness and invasive properties of cancer cells. For promotion of stemness, macrophages increase cancer cell HA production which upregulates stemness markers SOX2 and ALDH1A1 through PI3K-4EBP1 activation. Conversely, monocyte interaction with cancer cell VCAM-1 promotes CD44-VCAM-1 co-binding, inducing Ezrin/PI3K activation, and results in augmented cancer cell invasion. This is the first report to mechanistically describe a CD44-driven signaling switch from tumor initiation/growth to tumor invasion with TAM involvement in HNSCC.

MATERIALS AND METHODS

Patient tissue IHC analysis and quantification

Stained patient tissue slides were scanned and uploaded into Aperio eSlide Manager (Leica Biosystems, Wetzlar, Germany). Quantification of CD68/SOX2/ALDH1A1 brown/red relationship was performed using the Aperio ImageScope v12.3 program. Individual patient cases were opened in the software and zoomed all the way out (0.5x magnification) at which point only red staining could be detected by eye. For all 34 cases, 4–6 regions were selected; 2–3 areas with "high" red staining and 2–3 areas with "low" red staining (SOX2/ ALDH1A1). The regions were then zoomed to 20x magnification to detect brown (CD68) staining. Percent positive red was calculated for tumor tissue only, using an exclusion tool to remove any stroma or CD68 staining within the tumor. Likewise, percent positive brown staining was calculated for TAMs only, excluding any tumor tissue. Per patient case, mean SOX2/ALDH1A1 percentage staining was calculated for all selected regions. Values that fell above the mean were labeled "high" expression regions and values that fell below were labeled "low" expression regions. Corresponding percent CD68 values were plotted in GraphPad Prism 8.0 and t-test analyses performed. For quantifying "fade" at invasive tip, 2–

4 representative invasive edges were selected per patient case. Approximately equal areas (μm^2) were selected at the projecting invasive leading edge and at the root from where the invasive projection had stemmed and percent positive red was calculated. Root and leading edge values were normalized across cases. Values were plotted and compared using GraphPad Prism 8.0.

Cell lines

013C and 049C cell lines were established from patient-derived PDX tissue using RMK media [DMEM:F12 (3:1) with 10% FBS, Insulin (5μg/ml), EGF (10ng/ml), hydrocortisone (0.4 μg/ml), transferrin (5 μg/ml), penicillin (200units/mL), and streptomycin (200 ug/mL)] as previously described (9). Cell lines are routinely authenticated using DNA fingerprinting (STR analysis) and tested for *Mycoplasma* by the CU Molecular Biology Core Facility. STR analysis is confirmed with originating patient blood results. In general, cells used/passaged 30 times before fresh vial is thawed from authenticated batch for further use.

Sphere formation assays

Cells were plated in ultra-low attachment plates at a concentration of 2×10^5/well (6 well plate) or 1.0×10^4/well (96 well plate). Cells were allowed to form spheres for 8 days. For cell treatment and sphere formation assays, cells were treated with HA or anti-CD44 mAb on the day of seeding and again on day 3. Spheres were imaged, counted and measured using a Zeiss Axio Observer Z1 inverted microscope (Zeiss software Rel. 4.8). Experimental conditions were run in triplicate and experiments were repeated three times.

Isolation of primary human monocytes

Peripheral adult human blood was obtained from the University of Colorado Hospital Anschutz Medical Campus and peripheral blood mononuclear cells (PBMCs) isolated using density gradient centrifugation. The monocyte population was further isolated using the EasySep™ Human Monocyte Isolation Kit (#19359 StemCell Technologies, Vancouver, Canada). Isolated monocytes were plated in complete RPMI with 50 ng/mL M-CSF (Peprotech, New Jersey) and allowed to pre-differentiate into macrophages for 96 hours for activation of cytokine function and secretion prior to co-culture.

Co-culture assays

For suspended spheres, 2×10^5 cells/well were plated in ultra-low attachment plates (6-well plate) in 1.5 mL CSC media (9). On day 3, human monocytes were added to wells in 1.5 mL CSC media + 4% FBS (total well volume = 3 mL). For Matrigel spheres, 5×10^4 cells/well were plated (24-well plate) in CSC media in wells containing 300 μL of Matrigel (#356231 Corning, New York). On day 3, M-CSF exposed macrophages were added to wells in CSC media + 4% FBS. Experiments were repeated as needed (n   5) for flow cytometry and protein analysis via western blot (WB) and immunohistochemistry (IHC).

Proximity Ligation Assays (PLAs)

Spheroid slides were de-paraffinized, re-hydrated in graded alcohol concentrations, antigen retrieved by immersion in EDTA pH 9.0 [#S2367 Dako, (Agilent, Santa Clara, CA)], and

pressure cooked at 105 ºC for 20 min. The Duolink® *in situ* kit (Sigma-Aldrich, St. Louis, MO) in mouse/rabbit (with red detection) was used per the manufacturer's protocol (#DUO92002, 92004, 92008). Antibodies were 1:1,000 CD44 (#3570 Cell Signaling, Danvers, MA), 1:500 VCAM-1 (#ab134047 or #ab174279 (peptide-blockade treated spheres) (Abcam, Cambridge, United Kingdom), 1:200 Ezrin (#ab4069 Abcam), and 1:100 PIK3CA (#PA5-77798 Thermo Fisher, Waltham, MA). Slides were coverslipped using Fluoroshield Mounting Medium (#ab104135 Abcam) and dried overnight. Stacked images were taken using Zeiss Axio Observer Z1 inverted microscope (Zeiss software Rel. 4.8) and quantified using CellProfiler 2.2.0 software. Quantification of PLAs using CellProfiler described in supplemental methods.

shRNA experiments

CD44 silencing was completed using small hairpin RNA (shRNA) lentiviral constructs (sh#1: TCRN0000308110 and sh#2: TRCN0000296191) cloned into the pLKO.1 backbone, with the help of CU Cancer Center Functional Genomics Core. HEK 293T cells were transfected with LT1 reagent (Mirus) with scramble or CD44 sequences plus packaging plasmids per the supplier's instructions. Viral supernatant collected 48h post-transfection was applied to target cells for 24h. Infected cells were selected using puromycin (1.0μg/ml).

Mouse studies

Mouse SCC studies were previously described (26). Human CUHN013 xenograft tissue was harvested, chopped into 2–10mm^3 pieces, coated in Matrigel, and implanted into flanks and left shoulder of immunodeficient NOD *scid* gamma (NSG) mice (control/humanized) (27). When tumors reached 30–50mm^3, we performed intraperitoneal injections twice weekly for 4 weeks. Each experiment contained 2–6 mice per group, males and females were used in each study, mice were an average age of 6 months. Humanized mice used were humanized at an average age of 6–8 weeks. Treatment arms: 1) 200μL clodronate liposomes (5mg/mL) or control liposomes (Thermo Fisher), and 2) 1mg/kg anti-CD44 mAb or IgG isotype control (Creative Biolabs, Shirley, NY and Sigma-Aldrich).

Animal anesthesia and pain management

All procedures were approved by the University of Colorado IACUC. For cell injection and PDX tumor implantation animals were anesthetized with isoflurane (induction at 5%, maintained at 1–2%). In preparation for surgical tumor implantation/removal, and for 48h following the procedure, animals received buprenorphine injections (1mg/kg) every 12 h.

Study approval

Studies involving human subjects were approved by the Colorado Multiple Institutional Review Board (COMIRB-08-0552). Informed written consent was obtained from all patients whose tissues were used for this study. The University of Colorado Institutional Animal Care and Use Committee approved all mouse experiments.

Statistical analysis

In vitro and *in vivo* experiments were compared with two-group t-tests. Calculations were done using GraphPad Prism version 8.0. Data are represented graphically as mean ±SD unless noted. *P* < 0.05 were statistically significant. All statistical tests were two-sided.

Data and materials availability

Materials will be shared per the University of Colorado's Office for Technology Transfer policies and Institutional Review Board.

RESULTS

TAM distribution in the TME in HNSCC and link to CSC expression

CD44 is highly expressed across HNSCC tumors (Supplemental Fig. 1, top). Previously, we have shown regional variations in CSC distribution within HNSCCs, and how CSCs from different regions have distinct characteristics in terms of proliferative vs invasive potential, suggesting the importance of stromal influence on CSC function (28). Because TAMs are critical in HNSCC growth (26), we assessed their prevalence in HPV-positive and HPV-negative HNSCC patient samples and found TAM infiltration (measured by CD163 and CD68 staining), varied between regions of the same tumor (Supplemental Fig. 1, bottom). We used dual IHC staining to assess the relationship between TAM presence (CD68) with SOX2 and the Aldefluor surrogate ALDH1A1 expression (29). Out of 34 cases with detectable SOX2/ALDH1A1 expression, 28 demonstrated a TAM/CSC relationship, defined by a significant association between high TAM frequency and high SOX2/ALDH1A1 expression in non-invasive, rounded tumor edge regions (Fig. 1A–C, Supplemental Table 1). However, an opposing trend was observed with diminished SOX2/ALDH1A1 expression in the leading cells at projecting invasive edges with TAMs in close proximity (Fig. 1D, E).

Stemness and invasion are differentially promoted by PI3K signaling

To investigate TAM/cancer cell interactions, we developed two spheroid models by co-culturing early passage patient-derived HNSCC cells and human monocytes/macrophages. To model non-invasive tumor regions, we combined adherent Matrigel spheroids with differentiated human macrophages for cytokine secretion, mimicking a static or established TME (Fig. 2A left). A second spheroid model studied the invasive leading edge by combining non-adherent suspension spheroids with naïve human monocytes, mimicking a dynamic state actively recruiting TME components (Fig. 2A right). Because these relationships are more visually apparent in patient tumors with high SOX2 and ALDH1A1 expression, we used the CUHN013 cell line (013C) for model optimization. This cell line was derived from a patient tumor with high SOX2/ALDH1A1 expression resulting from the PI3K-4EBP1-SOX2 pathway (9).

In the static model of non-invasive areas, macrophages increased PI3K-4EBP1 phosphorylation in cancer cells, resulting in higher SOX2 (2-fold) and ALDH1A1 (3-fold) when compared to cancer cells cultured alone (Fig. 2B left, Fig. 2C left). Macrophage co-culture also increased the CSC population (ALDH$^+$CD44^{high}) and capacity for sphere formation compared to cancer alone (Fig. 2D, E). Given these findings and the prior

demonstration that PI3K-4EBP1-SOX2 signaling fosters CSC growth, we termed this the **cancer growth and proliferation (GP) co-culture model (co-culture[GP])**.

Conversely, in the invasive/suspension model, co-culture with monocytes resulted in reduced SOX2 (1.8-fold) and ALDH1A1 (1.5-fold) protein levels and decreased downstream PI3K-4EBP1 activation (Fig. 2B right, Fig. 2C right). This led to a diminished CSC fraction compared to cancer cells cultured without monocytes (alone[Inv]) (Fig. 2F). Notably, Zeb1, a known and reliable marker of invasive and mesenchymal HNSCC cells (Fig. 2G) (30), was increased by 4-fold in cancer cells in the co-culture[Inv] setting compared to alone[Inv] (Fig. 2H, Supplemental Fig. 2A). An additional marker of invasion, Vimentin, was further used to confirm this observation in patient tissue and the co-culture spheroid models (Supplemental Fig. 2B,C). Again, only the co-culture[Inv] spheres displayed significantly upregulated Vimentin compared to alone[Inv] (Supplemental Fig. 2C). Using a trans-well invasion assay, we observed increased invasion only when cancer cells were cultured in contact with monocytes, but not when monocytes were used as chemoattractant (Fig. 2I, Supplemental Fig. 2D). Thus, with this functional readout, we termed the spheroid model the **invasion co-culture model (co-culture[Inv])**.

HA-CD44 enriches the CSC population by regulating PI3K-4EBP1-SOX2 signaling

After establishing macrophage/monocyte influence on CSC expression and the PI3K-4EBP1-SOX2 pathway, we sought to determine the involvement of CD44. Interestingly, the flow data in Figure 2D demonstrated a change in CD44^{high} expressing cells. Elevated CD44 expression is known to be a marker of tumorigenic functions, particularly via ligand-binding with HA (11–15). Thus, we wanted to confirm the ligand binding role of CD44 in modulating the stemness pathway and whether HA binding to CD44 mediates the interactions between TAMs and cancer cells/CSCs. Addition of exogenous HA ligand increased the 013C CSC population, and inhibition of HA-binding (anti-CD44 mAb) reduced CSC numbers (Fig. 3A, B). Sphere formation increased with addition of HA in a dose-dependent manner, and was inhibited with addition of anti-CD44 mAb (Fig. 3C, D). HA-CD44 binding increased PI3K-4EBP1 activation, resulting in higher SOX2 expression (Fig. 3E, G). Conversely, anti-CD44 mAb ablated these effects and resulted in significantly reduced SOX2 (Fig. 3F, H).

We subsequently translated these observations to an *in vivo* model, using NSG mice bearing CUHN013 PDX tumors. Treatment with an anti-CD44 mAb resulted in significantly reduced tumor growth (Fig. 3I), in addition to suppression of the CSC population (Fig. 3J). To determine involvement of the PI3K-4EBP1-SOX2 pathway, IHC analysis was performed on control and treatment tumors. We found reduced PI3K-4EBP1-SOX2 expression in treated tumors compared to control (Fig. 3K, L), aligning with our *in vitro* studies. Overall, these results demonstrate that the HA-binding function of CD44 is critical in PI3K-4EBP1-SOX2 signaling and CSC maintenance (Fig. 3M).

TAMs mediate cancer cell HA production via CD44/HAS2 feedback loop

Cancer cells are known to be major contributors of HA in the TME (31). The CD44s (constant) isoform is associated with stem-like properties (32), and PI3K/Akt activation

resulting in upregulated HAS2 (33). HAS2 is the most important isoform in regulating tumor progression due to its HA synthesis function (34). Recently, CD44s-driven HAS2 upregulation has been shown to increase cancer cell HA production and promote HA-CD44 binding, establishing a HAS2/HA/CD44 positive feedback loop (33,34). Having observed HAS2 expression across HNSCC patient cases (Fig. 4A), we examined the HNSCC relevance of this established pathway *in vitro*. Knockdown of CD44 with shRNA significantly decreased HAS2 expression resulting in reduced HA production by cancer cells, as measured by HA ELISA (Fig. 4B, C). Reciprocally, when CD44s was over-expressed (OE), HAS2 expression significantly increased in spheres and enhanced HA production (Fig. 4D, E). To test the positive feedback of the HAS2/HA/CD44 loop, spheres treated with exogenous HA showed CD44s and HAS2 upregulation (Fig. 4F, G). Treatment of tumors *in vivo* with anti-CD44 mAb downregulated HAS2 expression (Fig. 4H). Further, increased cancer cell HA production by CD44s expression in turn led to upregulated PI3K-4EBP1-SOX2 activation (Fig. 4I).

To determine HA-CD44 involvement in macrophage-driven PI3K-4EBP1-SOX2 regulation, we tested if macrophages modulated cancer cell HA ligand availability through the above elucidated HAS2/HA/CD44 model (33). IHC of co-culture[GP] spheres showed higher CD44s and HAS2 compared to cancer alone spheres (Fig. 4J,K). Further, co-culture[GP] cancer cells had increased HA production versus cancer cells alone (Fig. 4L), suggesting macrophages promote stemness by increasing cancer cell HA availability via HAS2/HA/CD44 feedback. Overall, these findings support a HAS2/HA/CD44 positive feedback loop that modulates the PI3K-4EBP1-SOX2 pathway, and that macrophage-driven PI3K-4EBP1-SOX2 upregulation is aided by HA-CD44 (Fig. 4M).

TAMs influence CD44 expression and CSC regulation *in vivo*

We next sought to determine TAM influence on cancer cell CD44. To investigate TAM-driven changes in CD44 expression via TAM-secreted cytokines, we assessed IL-6, known for its roles in CD44 expression and TAM-mediated promotion of stemness (35,36). Macrophages flow-sorted from co-culture[GP] spheres had increased IL-6 production (Supplemental Fig. 3A). To ascertain if IL-6 exposure contributed to CD44s expression and signaling, cancer cells were exogenously treated with IL-6. This resulted in increased CD44s and HAS2 expression in addition to HA production (Supplemental Fig. 3B–D), suggesting macrophages may promote the HAS2/HA/CD44s feedback mechanism via IL-6. As we have shown that total CD44 is reduced in co-culture[Inv] setting (Fig. 2A, B right), we next showed that CD44 reduction decreased the CSC population as cell invasion increased (Supplemental Fig. 3E, F), supporting the observation that reduced CD44 expression promotes invasive signaling (37).

To test how TAM modulation influences tumor stemness *in vivo*, we depleted macrophages with liposomal clodronate in mice bearing murine SCC xenografts. Murine SCC models A223 and B931 are enriched in "side population" (SP) cells that efflux Hoechst dye, a defining characteristic of mouse SCC CSCs (26,38). These models were an ideal starting point due to their enriched CSC population; further, TAM ablation and tumor immune profiling for this model have been published (26). Clodronate reduced the SP population in

both models (Fig. 5A, B) and SP cells implanted into TAM-depleted mice exhibited diminished tumorigenicity (Fig. 5C). Finally, tumor SOX2 expression was suppressed in the treatment arm (Fig. 5D).

We conducted a TAM depletion study in a separate model with human HNSCC PDX tumors in NSG control and bone-marrow humanized mice (HM) to confirm TAM-aided CSC maintenance (27). We confirmed that clodronate reduced spleen and tumor mouse macrophage (NSG and HM) and human macrophage (HM) populations compared to control mice (Supplemental Fig. 4A–D). Interestingly, although both groups of mice had reduced mouse TAM populations, only the HM tumors demonstrated a significant decrease in CSCs (Fig. 5E). Human TAM depletion reduced tumor growth in clodronate treated HM by 25% and 42% when compared to control HM and clodronate-treated NSG mice, respectively (Fig. 5F). Further, only tumors from clodronate-treated HM had reduced SOX2 expression (Fig. 5G). These data suggest species-specificity in cancer cell-TME interactions. Both mouse and human HNSCC models supported TAM-mediated stemness and growth-promoting effect.

CD44-VCAM-1 drives monocyte-influenced HNSCC cell invasion

We next sought to understand the mechanism for TAM-mediated invasion. In breast cancer, monocyte binding to the CD44 partner VCAM-1 leads to activation of Ezrin, and subsequent promotion of PI3K/Akt invasive signaling (39,40). In co-culture[Inv] conditions, VCAM-1 was augmented in HNSCC cells (Fig. 6A, B) alongside Ezrin phosphorylation when compared to HNSCC alone[Inv] (Fig. 6C). To determine CD44 involvement in this invasive signaling and confirm this pathway is occurring in HNSCCs, we used proximity ligation assays (PLAs) to verify protein-protein interactions. CD44 interaction with VCAM-1, Ezrin association with VCAM-1, and Ezrin recruitment of PI3K all increased by PLA in co-culture[Inv] spheres (Fig. 6D). Notably, increased CD44-VCAM-1 interactions do not occur in the co-culture[GP] model (Fig. 6E). To verify these associations are responsible for the invasive phenotype, we blocked monocyte binding to VCAM-1 with a blocking peptide. This abolished increased cancer cell invasion (Fig. 6F), decreased the CD44-VCAM-1 associations by PLA (Fig. 6G), and rescued CSC enrichment in co-culture[Inv] conditions (Fig. 6H). Furthermore, we confirmed VCAM-1 associated with invasion across representative patient cases (Fig. 6I), supporting validity of the *in vitro* studies. We propose that CD44-VCAM-1 interaction leads to invasion due to a shift from the PI3K-4EBP1-SOX2 pathway and towards an Ezrin-PI3K pathway (Fig. 6J). These data suggest the two phenotypes (growth- and invasion-promoting) are supported by CD44-driven activation of PI3K/Akt (per Fig. 2A), but subsequently diverge in their downstream signaling to enable two outcomes.

HA serves as the link between growth- and invasion-promoting pathways

HA-CD44 binding can also promote cancer cell migration and invasion (14). Because we demonstrated that HA promotes stemness and growth via CD44-PI3K-4EBP1-SOX2 (Fig. 3), we next examined the importance of HA in promoting invasion. We demonstrate that HA ligand increased cancer cell invasion in a dose-response manner and that inhibition of HA binding with anti-CD44 ablated this effect (Supplemental Fig. 5A,B). To test if HA promotes the expression of key co-culture[Inv] markers (Zeb1 and VCAM-1), we analyzed

spheres treated with exogenous HA; both have increased protein expression by HA (Supplemental Fig. 5C–E).

The growth and invasion data suggest that HA could serve as a functional link between the two models; first promoting epithelial-driven growth, yet also setting the stage for invasion. We hypothesized that the co-culture[GP] model represents an early stage model. As tumor growth is aided by HA, a CD44 signaling change is triggered to subsequently promote an invasive phenotype (mimicked by the co-culture[Inv] model) (Supplemental Fig. 6A). Interestingly, transitional edges (with non-invasive and invasive features) were observed in patient tissue (Supplemental Fig. 6B). Given SOX2's importance in HNSCC tumorigenicity (9), we tested its role in monocyte/macrophage recruitment to aid in further tumor progression (Supplemental Fig. 6C). SOX2 over-expressing 013C increased sphere interaction with monocytes and the number of monocytes recruited per sphere (Supplemental Fig. 6D–F). To test the two-stage hypothesis *in vivo*, we implanted CUHN013 PDX into NSG and HM mice and collected tumors at 'small' and 'large' stages of growth, (50–100mm^3 and 150–250mm^3, respectively) (Supplemental Fig. 6G). Small HM tumors had more CSCs versus small NSG tumors, mirroring the co-culture[GP] CSC phenotype (Supplemental Fig. 6H, Fig. 2C), and that large HM tumors contained fewer CSCs compared to large NSG tumors, mirroring the co-culture[Inv] CSC phenotype (Supplemental Fig. 6H, Fig. 2F). SOX2 IHC expression correlated with CSC populations and sphere models only in HM tumors (Supplemental Fig. 6I).

We previously demonstrated the invasive potential of CUHN013 PDXs lies at the tumor edge (28). As seen in the co-culture[Inv] model, VCAM-1 had higher expression at the edge in both NSG and HM tumors (Supplemental Fig. 6J). Only HM tumors, however, displayed decreased SOX2 expression at the edges (Supplemental Fig. 6K), resembling the SOX2 "fade" depicted in Fig. 1D. Overall, the HM platform mirrored TME heterogeneity seen in patient tumors and confirmed a phenotypic switch that hinges upon the presence of species-specific macrophages/monocytes.

CD44 shift via Zeb1/ESRP1 feedback regulates the growth-to-invasion switch

We next sought to determine how such a switch in signaling could occur. Epithelial splicing regulatory protein 1 (ESRP1) and Zeb1 regulate epithelial-to-mesenchymal plasticity and CD44 isoform expression in HNSCC (14,41). Therefore, we analyzed expression of Zeb1, ESRP1, CD44v10, and CD44s to reveal striking differences between the two model systems (Fig. 7A). The spheres[GP] had higher ESRP1 and ESRP1-promoted CD44v8–10 expression suggesting an epithelial-like phenotype (41) (Fig. 7A, Supplemental Fig. 7A, D). Conversely, the spheres[Inv] had diminished ESRP1/CD44v10 expression and elevated CD44s and Zeb1, suggesting a mesenchymal-like phenotype (Fig. 7A, Supplemental Fig. 7A–D). To determine functional CD44 isoform differences that could explain the opposing phenotypes in our models, we overexpressed CD44s and CD44v8-10 in HNSCC cells with opposite CD44 expression patterns (Supplemental Fig. 7E) and tested cancer cell sphere formation and invasion. CD44v8-10 expression dramatically increased sphere formation in both cell lines (Fig. 7B), while CD44s augmented cancer cell invasion (Fig. 7C).

Given ESRP1 loss increases cancer cell motility and occurs at the invasive edges of SCC patient tumors (41), we tested patient samples to verify the CD44 expression switch. Indeed, when comparing non-invasive to invasive edges, the leading edge of invasive projections displayed lowered ESRP1, increased Zeb1, maintained CD44s, and lowered CD44v10 expression compared to non-invasive edges (Fig. 7D). Combined, these data suggest different functional phenotypes emerge due to prevailing CD44 isoform expression, that the growth- and invasion-promoting signaling mechanisms are regulated by a CD44 switch, and its regulation can be influenced by the TME and HA exposure (Fig. 7E).

DISCUSSION

In this study, we explored the mechanistic underpinnings of the associations between TAMs and CSCs that we originally observed in HNSCC patient tissues. Using *in vitro* co-culture spheroid and *in vivo* mouse models, we identified TAM influence on CSC function was dependent on HA-CD44 interaction, CD44 isoform expression, and PI3K-4EBP1-SOX2 signaling activation. We revealed a two-stage sequence representing the continuum of tumor growth and invasion as it exists in patient tumors. In the first step, we demonstrate a tumor growth-promoting relationship where the presence of TAMs upregulates HA-CD44 interaction via HAS2, resulting in increased stemness via PI3K-4EBP1-SOX2 signaling activation and increased epithelial CSC capabilities. In the second step, we demonstrate monocyte recruitment increased cancer cell invasive potential through monocyte-activated CD44-VCAM-1 binding, leading to diminished PI3K-4EBP1-SOX2 signaling, reduced SOX2 and ALDH1A1, and increased Zeb1. Blocking monocyte-cancer interaction reversed the invasive phenotype to the growth-promoting phenotype, linking both mechanisms. Finally, we note how CD44 expression changes and regulation via Zeb1/ESRP1 could explain TAM-influenced cancer cell plasticity.

Previous studies have demonstrated the importance of HA-CD44 interaction and associated signaling for promotion of stem-like abilities across tumor types (12,42,43). This interaction has been linked to overall disease progression and poor prognosis (14). We affirmed that this HA-CD44 relationship remains true in HNSCC models, and also established it as an upstream regulator of the PI3K-4EBP1-SOX2 pathway in CSCs, previously unknown. These data also link the HA-CD44 interaction with promotion of HAS2 expression and HA production, supporting a recently established positive feedback loop by Lie et al. (33). Notably, cancer cell HA production via HAS2 promotes tumor progression in a CD44-dependent manner (44). Further, the importance of HA in the TME has expanded to reveal that HA serves a dual nature by promoting cancer initiation while also aiding in invasion and resistance (31,34). Our study expands on this idea by demonstrating that HA can influence both growth and invasion of HNSCCs, suggesting HA promotes one phenotype while also setting the stage for the emergence of others.

In addition to being a principal receptor for HA, CD44 can have many binding partners to serve its multifunctional purposes (14). VCAM-1 is an emerging target of cancer cell progression and invasion (45), and regulates CD44 expression (35). Monocyte binding to VCAM-1 promotes breast cancer invasion and CD44-VCAM-1 partnering induces malignant cancer cell signaling (39,40). However, the question remained as to whether these

two mechanisms were connected. We found monocyte presence increased VCAM-1 expression, activated Ezrin-PI3K signaling, and increased HNSCC invasion. We also determined CD44-VCAM-1 association was exclusive to the invasive phenotype, connecting these two mechanisms in HNSCC. The signaling pathway downstream of Ezrin-PI3K that contributes to this invasive action, however, remains to be elucidated. Overall, given the role of PI3K signaling in both the growth and invasion phenotypes, the future investigations of how PI3K inhibitors modulate TAM interactions *in vivo* may provide insight into its therapeutic potential.

CD44 variant-switching has recently been shown to determine tumor progression (15,19,46), and impact clinical outcomes (32,47). The regulation of CD44 is complex (35), and CD44 participates in a Zeb1/ESRP1/HAS2/CD44 regulatory feedback loop promoting progression and plasticity (48). ESRP1, highly expressed in cells with an epithelial phenotype, inhibits epithelial-to-mesenchymal transition (EMT) by promoting CD44v expression over CD44s. On the other hand, expression of Zeb1 transcriptionally represses ESRP1, promoting high CD44s expression and inducing EMT (14). Our data suggest a CD44-controlled switch between the stemness/growth-promoting and invasion-promoting phenotypes. Further delineation of specific contributions from each CD44v isoform is a focus of future studies.

Most critically, however, it has been shown that CD44 expression and function are influenced by reciprocal interactions between cancer cells, CSCs and TAMs (17–19). These findings confirm the role of CD44 as a mediator between TAMs and CSCs; we are the first to demonstrate this CD44/TAM interplay in HNSCC. These data not only demonstrate TAM influence on CD44 signaling directly via ligand binding, but also indicate that TAM presence can influence CD44 function indirectly playing a role in modulating regulators of CD44 expression, such as Zeb1 (49) and VCAM-1. Taken together, we propose a complete mechanistic model for how the phenotypic switch may occur (Fig. 7E).

We acknowledge that our study has limitations, and whereas the focus of this report is TAM modulation of the PI3K-4EBP1-SOX2 pathway via HA-CD44, we recognize that the phenotypic switch entails additional concurrent signaling changes and activity by transcriptional regulators not addressed here. Further, we note that TAM contribution to the TME and CSC stemness is multifaceted, with a multitude of secreted factors at play in addition to IL-6. Our current study provides an initial model of a likely more complex TAM/CSC network. Ongoing and future studies are aimed at dissecting this complex interplay, including how secreted factors, such as IL-6, influence CD44 expression and function in addition to how other cell-cell interactions could be involved.

In summary, TAMs are key in promoting cancer progression across tumor types, particularly by promoting stemness. How TAMs and CSCs communicate in order to fulfill these functions remains largely unknown in HNSCC and it is critical to define the molecular mechanisms underlying such crosstalk. Given that TAMs are also critical in therapy resistance and poor prognosis (25,50), understanding mechanistic links between these key players, intrinsically and extrinsically to the cancer cell, could be a vital area of focus for target and drug discovery.

Author Manuscript

Author Manuscript

Author Manuscript

Author Manuscript

Supplementary Material

Refer to Web version on PubMed Central for supplementary material.

Acknowledgements

References

1. Jemal A, Siegel R, Ward E, Hao Y, Xu J, Murray T, et al. Cancer Statistics, 2008. CA: A Cancer Journal for Clinicians 2008;58:71–96 [PubMed: 18287387]

2. Siegel RL, Miller KD, Jemal A. Cancer statistics, 2018. CA: A Cancer Journal for Clinicians 2018;68:7–30 [PubMed: 29313949]

3. Chaturvedi AK, Engels EA, Anderson WF, Gillison ML. Incidence Trends for Human Papillomavirus–Related and –Unrelated Oral Squamous Cell Carcinomas in the United States. Journal of Clinical Oncology 2008;26:612–9 [PubMed: 18235120]

4. Chaturvedi AK, Engels EA, Pfeiffer RM, Hernandez BY, Xiao W, Kim E, et al. Human Papillomavirus and Rising Oropharyngeal Cancer Incidence in the United States. Journal of Clinical Oncology 2011;29:4294–301 [PubMed: 21969503]

5. Ailles LE, Weissman IL. Cancer stem cells in solid tumors. Current Opinion in Biotechnology 2007;18:460–6 [PubMed: 18023337]

6. Prince MEP, Ailles LE. Cancer Stem Cells in Head and Neck Squamous Cell Cancer. Journal of Clinical Oncology 2008;26:2871–5 [PubMed: 18539966]

7. Maitland NJ, Collins AT. Cancer stem cells - A therapeutic target? Curr Opin Mol Ther 2010;12:662–73 [PubMed: 21154158]

8. Bourguignon LYW, Wong G, Earle C, Chen L. Hyaluronan-CD44v3 interaction with Oct4-Sox2-Nanog promotes miR-302 expression leading to self-renewal, clonal formation, and cisplatin resistance in cancer stem cells from head and neck squamous cell carcinoma. J Biol Chem 2012;287:32800–24 [PubMed: 22847005]

9. Keysar SB, Le PN, Miller B, Jackson BC, Eagles JR, Nieto C, et al. Regulation of Head and Neck Squamous Cancer Stem Cells by PI3K and SOX2. JNCI: Journal of the National Cancer Institute 2016;109

10. Plaks V, Kong N, Werb Z. The Cancer Stem Cell Niche: How Essential Is the Niche in Regulating Stemness of Tumor Cells? Cell Stem Cell 2015;16:225–38 [PubMed: 25748930]

11. Thapa R, Wilson GD. The Importance of CD44 as a Stem Cell Biomarker and Therapeutic Target in Cancer. Stem Cells International 2016;2016:15

12. Skandalis SS, Karalis TT, Chatzopoulos A, Karamanos NK. Hyaluronan-CD44 axis orchestrates cancer stem cell functions. Cell Signal 2019;63:109377 [PubMed: 31362044]

13. Yan Y, Zuo X, Wei D. Concise Review: Emerging Role of CD44 in Cancer Stem Cells: A Promising Biomarker and Therapeutic Target. STEM CELLS Translational Medicine 2015;4:1033–43 [PubMed: 26136504]

14. Chen C, Zhao S, Karnad A, Freeman JW. The biology and role of CD44 in cancer progression: therapeutic implications. Journal of Hematology & Oncology 2018;11 [PubMed: 29357914]

15. Zhao S, Chen C, Chang K, Karnad A, Jagirdar J, Kumar AP, et al. CD44 Expression Level and Isoform Contributes to Pancreatic Cancer Cell Plasticity, Invasiveness, and Response to Therapy. Clin Cancer Res 2016;22:5592–604 [PubMed: 27267855]

16. Chanmee T, Ontong P, Konno K, Itano N. Tumor-Associated Macrophages as Major Players in the Tumor Microenvironment. Cancers 2014;6:1670–90 [PubMed: 25125485]

17. Rao G, Wang H, Li B, Huang L, Xue D, Wang X, et al. Reciprocal Interactions between Tumor-Associated Macrophages and CD44-Positive Cancer Cells via Osteopontin/CD44 Promote Tumorigenicity in Colorectal Cancer. Clinical Cancer Research 2013;19:785–97 [PubMed: 23251004]

18. Ma C, Komohara Y, Ohnishi K, Shimoji T, Kuwahara N, Sakumura Y, et al. Infiltration of tumor-associated macrophages is involved in CD44 expression in clear cell renal cell carcinoma. Cancer Science 2016;107:700–7 [PubMed: 26918621]

19. Yang C, Cao M, Liu Y, He Y, Du Y, Zhang G, et al. Inducible formation of leader cells driven by CD44 switching gives rise to collective invasion and metastases in luminal breast carcinomas. Oncogene 2019;38:7113–32 [PubMed: 31417182]

20. Sainz B Jr., Carron E, Vallespinós M, Machado HL. Cancer Stem Cells and Macrophages: Implications in Tumor Biology and Therapeutic Strategies. Mediators Inflamm 2016;2016:9012369 [PubMed: 26980947]

21. Jinushi M, Chiba S, Yoshiyama H, Masutomi K, Kinoshita I, Dosaka-Akita H, et al. Tumor-associated macrophages regulate tumorigenicity and anticancer drug responses of cancer stem/initiating cells. Proceedings of the National Academy of Sciences 2011;108:12425

22. Yang J, Liao D, Chen C, Liu Y, Chuang T-H, Xiang R, et al. Tumor-Associated Macrophages Regulate Murine Breast Cancer Stem Cells Through a Novel Paracrine EGFR/Stat3/Sox-2 Signaling Pathway. STEM CELLS 2013;31:248–58 [PubMed: 23169551]

23. Siegle JM, Basin A, Sastre-Perona A, Yonekubo Y, Brown J, Sennett R, et al. SOX2 is a cancer-specific regulator of tumour initiating potential in cutaneous squamous cell carcinoma. Nature Communications 2014;5

24. Boumahdi S, Driessens G, Lapouge G, Rorive S, Nassar D, Le Mercier M, et al. SOX2 controls tumour initiation and cancer stem-cell functions in squamous-cell carcinoma. 2014;511:246–50

25. He K-F, Zhang L, Huang C-F, Ma S-R, Wang Y-F, Wang W-M, et al. CD163+ Tumor-Associated Macrophages Correlated with Poor Prognosis and Cancer Stem Cells in Oral Squamous Cell Carcinoma. BioMed Research International 2014;2014:1–9

26. Wu FL, Nolan K, Strait AA, Bian L, Nguyen KA, Wang JH, et al. Macrophages Promote Growth of Squamous Cancer Independent of T cells. Journal of Dental Research 2019;98:896–903 [PubMed: 31189369]

27. Morton JJ, Keysar SB, Perrenoud L, Chimed T-S, Reisinger J, Jackson B, et al. Dual use of hematopoietic and mesenchymal stem cells enhances engraftment and immune cell trafficking in an allogeneic humanized mouse model of head and neck cancer. Mol Carcinog 2018;57:1651–63 [PubMed: 30129680]

28. Chowdhury FN, Reisinger J, Gomez KE, Chimed T-S, Thomas CM, Le PN, et al. Leading edge or tumor core: Intratumor cancer stem cell niches in oral cavity squamous cell carcinoma and their association with stem cell function. Oral Oncology 2019;98:118–24 [PubMed: 31586893]

29. Rasheed ZA, Yang J, Wang Q, Kowalski J, Freed I, Murter C, et al. Prognostic significance of tumorigenic cells with mesenchymal features in pancreatic adenocarcinoma. J Natl Cancer Inst 2010;102:340–51 [PubMed: 20164446]

30. Keysar SB, Le PN, Anderson RT, Morton JJ, Bowles DW, Paylor JJ, et al. Hedgehog Signaling Alters Reliance on EGF Receptor Signaling and Mediates Anti-EGFR Therapeutic Resistance in Head and Neck Cancer. Cancer Research 2013;73:3381 [PubMed: 23576557]

31. Liu M, Tolg C, Turley E. Dissecting the Dual Nature of Hyaluronan in the Tumor Microenvironment. Frontiers in Immunology 2019;10 [PubMed: 30723470]

32. Bhattacharya R, Mitra T, Ray Chaudhuri S, Roy SS. Mesenchymal splice isoform of CD44 (CD44s) promotes EMT/invasion and imparts stem-like properties to ovarian cancer cells. Journal of Cellular Biochemistry 2018;119:3373–83 [PubMed: 29130517]

33. Liu S, Cheng C. Akt Signaling Is Sustained by a CD44 Splice Isoform–Mediated Positive Feedback Loop. Cancer Research 2017;77:3791–801 [PubMed: 28533273]

34. Passi A, Vigetti D, Buraschi S, Iozzo RV. Dissecting the role of hyaluronan synthases in the tumor microenvironment. The FEBS Journal 2019;286:2937–49 [PubMed: 30974514]

35. Xu H, Tian Y, Yuan X, Wu H, Liu Q, Pestell RG, et al. The role of CD44 in epithelial-mesenchymal transition and cancer development. Onco Targets Ther 2015;8:3783–92 [PubMed: 26719706]

36. Wan S, Zhao E, Kryczek I, Vatan L, Sadovskaya A, Ludema G, et al. Tumor-associated macrophages produce interleukin 6 and signal via STAT3 to promote expansion of human hepatocellular carcinoma stem cells. Gastroenterology 2014;147:1393–404 [PubMed: 25181692]

37. Chetty C, Vanamala SK, Gondi CS, Dinh DH, Gujrati M, Rao JS. MMP-9 induces CD44 cleavage and CD44 mediated cell migration in glioblastoma xenograft cells. Cell Signal 2012;24:549–59 [PubMed: 22024282]

38. White RA, Neiman JM, Reddi A, Han G, Birlea S, Mitra D, et al. Epithelial stem cell mutations that promote squamous cell carcinoma metastasis. Journal of Clinical Investigation 2013;123:4390–404

39. Chen Q, Zhang Xiang HF, Massagué J. Macrophage Binding to Receptor VCAM-1 Transmits Survival Signals in Breast Cancer Cells that Invade the Lungs. Cancer Cell 2011;20:538–49 [PubMed: 22014578]

40. Wang P-C, Weng C-C, Hou Y-S, Jian S-F, Fang K-T, Hou M-F, et al. Activation of VCAM-1 and Its Associated Molecule CD44 Leads to Increased Malignant Potential of Breast Cancer Cells. International Journal of Molecular Sciences 2014;15:3560–79 [PubMed: 24583847]

41. Ishii H, Saitoh M, Sakamoto K, Kondo T, Katoh R, Tanaka S, et al. Epithelial splicing regulatory proteins 1 (ESRP1) and 2 (ESRP2) suppress cancer cell motility via different mechanisms. J Biol Chem 2014;289:27386–99 [PubMed: 25143390]

42. Ohno Y, Shingyoku S, Miyake S, Tanaka A, Fudesaka S, Shimizu Y, et al. Differential regulation of the sphere formation and maintenance of cancer-initiating cells of malignant mesothelioma via CD44 and ALK4 signaling pathways. Oncogene 2018;37:6357–67 [PubMed: 30061637]

43. Bourguignon LYW, Earle C, Wong G, Spevak CC, Krueger K. Stem cell marker (Nanog) and Stat-3 signaling promote MicroRNA-21 expression and chemoresistance in hyaluronan/CD44-activated head and neck squamous cell carcinoma cells. Oncogene 2012;31:149–60 [PubMed: 21685938]

44. Wang SJ, Earle C, Wong G, Bourguignon LYW. Role of hyaluronan synthase 2 to promote CD44-dependent oral cavity squamous cell carcinoma progression. Head & Neck 2013;35:511–20

45. Kong DH, Kim YK, Kim MR, Jang JH, & Lee S Emerging Roles of Vascular Cell Adhesion Molecule-1 (VCAM-1) in Immunological Disorders and Cancer. International Journal of Molecular Sciences 2018;19:1057

46. Brown RL, Reinke LM, Damerow MS, Perez D, Chodosh LA, Yang J, et al. CD44 splice isoform switching in human and mouse epithelium is essential for epithelial-mesenchymal transition and breast cancer progression. 2011;121:1064–74

47. Athanassiou-Papaefthymiou M, Shkeir O, Kim D, Divi V, Matossian M, Owen JH, et al. Evaluation of CD44 variant expression in oral, head and neck squamous cell carcinomas using a triple approach and its clinical significance. Int J Immunopathol Pharmacol 2014;27:337–49 [PubMed: 25280025]

48. Jolly MK, Preca B-T, Tripathi SC, Jia D, George JT, Hanash SM, et al. Interconnected feedback loops among ESRP1, HAS2, and CD44 regulate epithelial-mesenchymal plasticity in cancer. APL Bioeng 2018;2:031908 [PubMed: 31069317]

49. Preca B-T, Bajdak K, Mock K, Lehmann W, Sundararajan V, Bronsert P, et al. A novel ZEB1/ HAS2 positive feedback loop promotes EMT in breast cancer. 2017

50. Balermpas P, Rödel F, Liberz R, Oppermann J, Wagenblast J, Ghanaati S, et al. Head and neck cancer relapse after chemoradiotherapy correlates with CD163+ macrophages in primary tumour

and CD11b+ myeloid cells in recurrences. British Journal of Cancer 2014;111:1509–18 [PubMed: 25093488]

SIGNIFICANCE

Findings establish a mechanistic link between tumor cell CD44, TAM, and CSC properties at the tumor-stroma interface that can serve as a vital area of focus for target and drug discovery.
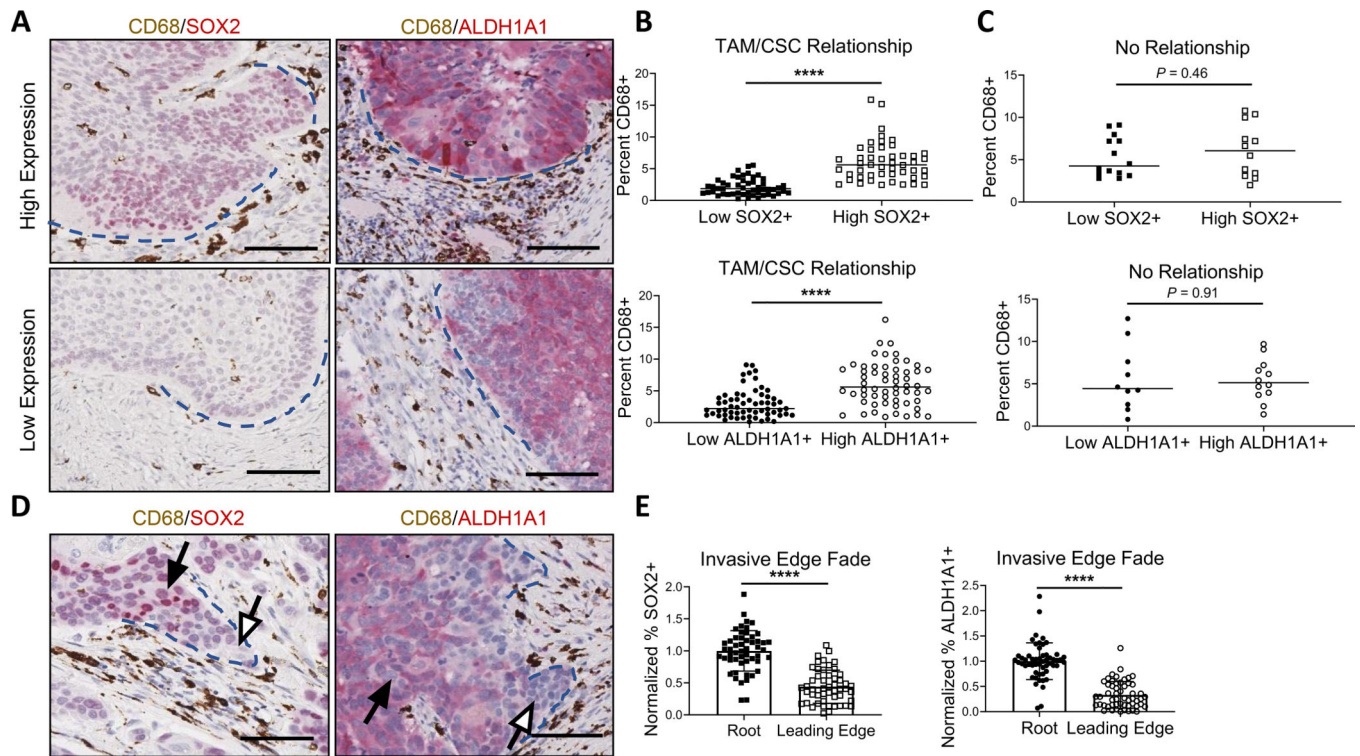
Figure 1. TAM presence at non-invasive and invasive edges correlates with altered CSC marker expression.

(**A**) Representative images (20x) of high SOX2 and high ALDH1A1 (top) and low SOX2 and low ALDH1A1 (bottom) regions (red) with associated TAM presence (CD68, brown). Blue dashed lines indicate rounded, non-invasive tumor edge. (**B**) Regions with high SOX2 (top) and high ALDH1A1 (bottom) expression contained significantly higher TAM presence (n = 28 patient cases). (**C**) No relationship between TAM presence and SOX2 (top) or ALDH1A1 (bottom) observed in remaining cases (n = 6 patient cases). (**D**) Invasive edge representative images of SOX2 (left) or ALDH1A1 (right) with associated TAM presence. Blue dashed lines indicate projecting tumor edge. White arrows point to faded leading edge and black arrows point to corresponding "root". (**E**) Quantified drop in SOX2 (left) and ALDH1A1 (right) expression at leading edge compared to root (n = 20 patient cases). Quantification was done using Aperio ImageScope v12.3 software. ****P<0.0001, 2-tailed unpaired Student's *t* test. (**A**, **D**) Scale bars: 100μm.
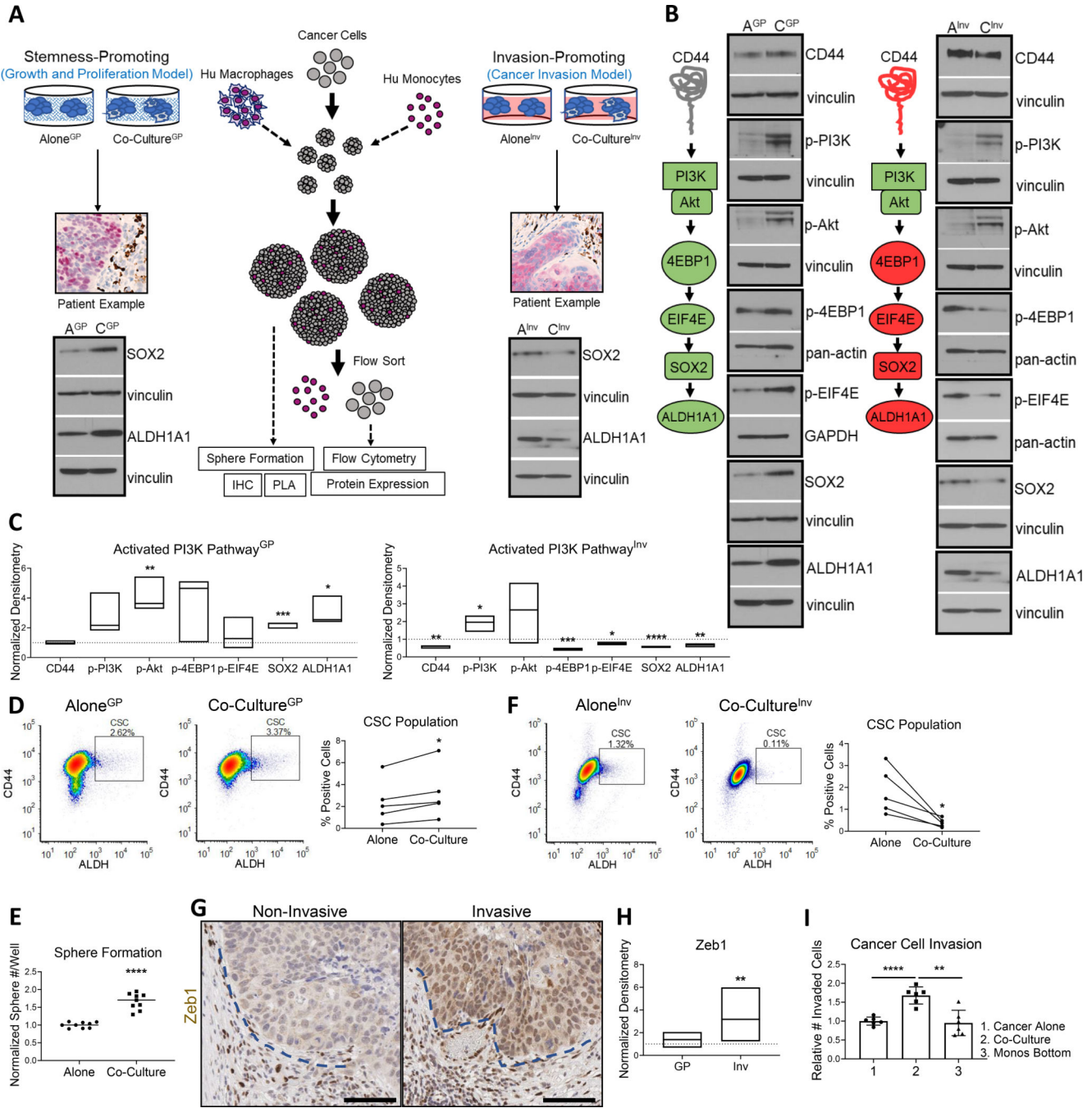
Figure 2. Human macrophage/monocyte effects on PI3K-4EBP1-SOX2 signaling for promotion of growth or invasion.

(**A**) Left, the growth-promoting relationship between TAMs and cancer cells was modeled using spheroids grown in Matrigel to mimic the 3D tissue setting. For cytokine function/ secretion, pre-differentiated macrophages were added to spheres in their early days of culture. Right, the invasion-promoting relationship between TAMs and cancer cells was modeled using spheroids grown in suspension to mimic lowered cell adhesion. Isolated monocytes used were naïve monocytes for cancer cell recruitment for aid in intravasation and extravasation. WB below each model depicts CSC protein levels in co-culture setting are

representative of the relationship visualized in patient tissue. (**B**) Left, representative WB diagram of PI3K-4EBP1-SOX2 activation resulting in increased SOX2 and ALDH1A1 protein expression. Right, representative WB diagram of decreased downstream PI3K-4EBP1-SOX2 activation, decreasing SOX2 and ALDH1A1 protein expression. GP = growth and proliferation model, Inv = invasion model, A = cancer cells alone, C = cancer cells co-cultured. Vinculin, pan-actin, and GAPDH used as loading controls. (**C**) Left, floating bar plot of normalized WB densitometry for GP model. Right, for Inv model. Line at y = 1 represents protein expression of cancer cells alone. (**D**) Macrophage presence increased percent CSCs. Left, representative flow diagrams. Right, paired line plot demonstrating increase across repeats (n=5). (**E**) Macrophages increased sphere formation of cancer cells. Three wells plated per repeat and 3 repeats performed. (**F**) Monocyte presence decreased percent CSCs. Left, representative flow diagrams. Right, paired line plot demonstrating decrease across repeats (n=5). (**G**) Representative patient tissue with Zeb1 expression at non-invasive and invasive tumor edges indicated by blue dotted lines, respectively. (**H**) Floating bar plot of normalized WB densitometry for Zeb1 expression in both models. (**I**) Cancer cell invasion with monocyte co-culture or with monocytes used as lure (monos bottom). Two wells per repeat and 3 repeats performed. WB densitometry in **C** and **H** based on quantification of 3 separate repeats. Statistical significance in **C**, **E**, **H**, and **I** determined by 2-tailed unpaired Student's t test. **D** and **F** statistics determined by 2-tailed paired Student's t test *P<0.05, **P<0.01, ***P<0.001, ****P<0.0001.
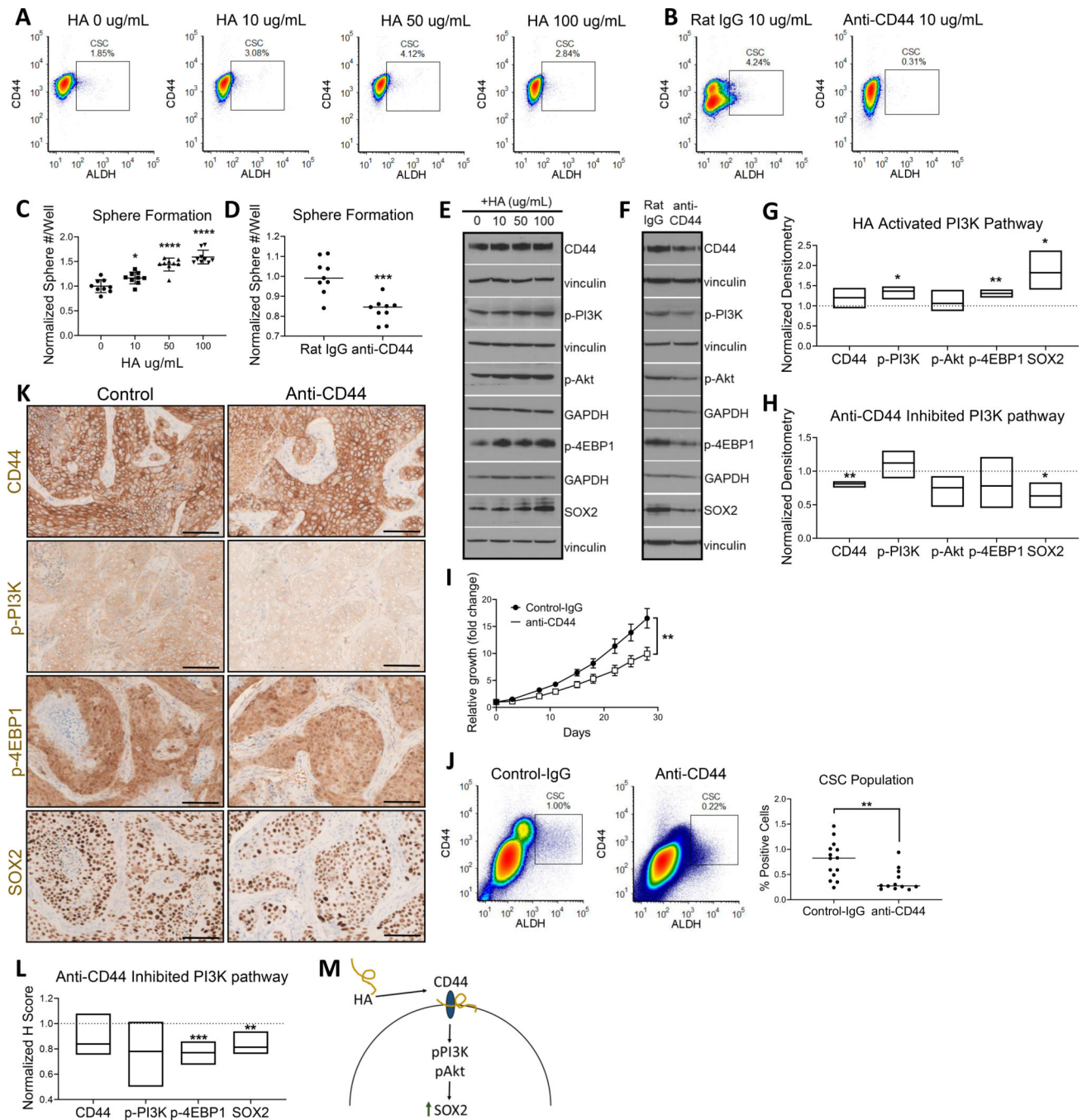
Figure 3. HA-CD44 promotes stemness via PI3K-4EBP1-SOX2 pathway activation.
(**A**) HA treatment increased the percent CSC population as measured via flow cytometry.
(**B**) HA binding blockade with anti-CD44 mAb decreased percent CSC population. (**C**)
Cancer cell sphere formation increased with increasing doses of HA. (**D**) Cancer cell sphere
formation decreased with ligand blockade. (**E**) WB of activated PI3K-4EBP1-SOX2
pathway with HA treatment. (**F**) WB of lowered PI3K-4EBP1-SOX2 pathway activation
with anti-CD44 mAb treatment. For **E** and **F**, vinculin and GAPDH were used as loading
controls. (**G**) Floating bar plot of normalized WB densitometry of 3 repeats for 50μg/mL

HA. Line at y = 1 represents protein expression of 0μg/mL HA control. (**H**) Floating bar plot of normalized WB densitometry of 3 repeats. Line at y = 1 represents protein expression of treatment with Rat IgG isotype control. (**I**) *In vivo* treatment of NSG mice with anti-CD44 mAb results in reduced tumor growth. Tumor growth curve (top) and final tumor size comparison (bottom) (IgG = 14 tumors, anti-CD44 = 12 tumors). (**J**) *In vivo* treatment of NSG mice with anti-CD44 mAb results in decreased percent CSC population. (**K**) *In vivo* treatment with anti-CD44 mAb decreases CD44-pPI3K-p4EBP1-SOX2 tumor expression (**L**) Normalized H score of anti-CD44 treated tumor IHC. Line at y = 1 represents average H score of control tumors (n = 6 tumors each). (**M**) Mechanistic overview of promotion of PI3K-4EBP1-SOX2 pathway signaling due to CD44 ligand binding. For **C** and **D**, 3 wells plated per repeat and 3 repeats performed. Statistical significance in **C**, **D**, **G**, **H**, **I** and **J** determined by 2-tailed unpaired Student's *t* test $*P<0.05$, $**P<0.01$, $***P<0.001$, $****P<0.0001$. Scale bars: 100μm.
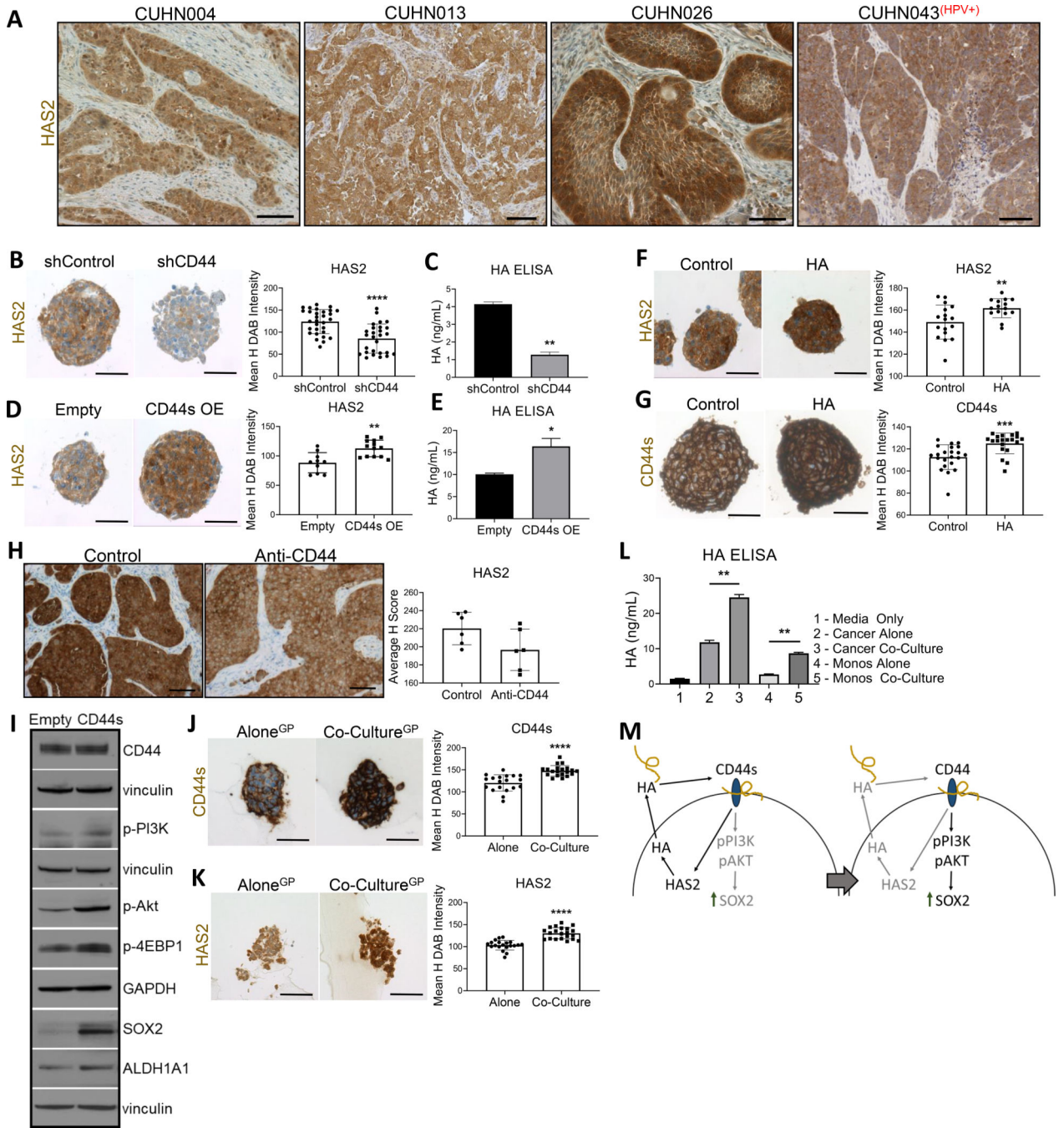
Figure 4. CD44s drives HAS2/HA/CD44 pathway and promotes PI3K signaling.
(**A**) Representative images of HAS2 (brown) expression of tumor cells. For **B**, **D**, **F**, **G**, **J**, and **K**: left, representative sphere IHC images; right, mean H DAB staining intensity quantification of one representative repeat, n = # spheres quantified. (**B**) Knockdown of CD44 decreased HAS2 expression (shControl n = 30, shCD44 (#1 and #2 data combined, n = 27). (**C**) Reduced HAS2 expression by CD44 knockdown resulted in decreased HA production by cancer cells as measured by HA ELISA. (**D**) Overexpression of CD44s isoform increased HAS2 expression (empty n = 10, CD44s n = 12). (**E**) CD44s induced

HAS2 resulted in increased HA production by cancer cells. (**F**) HA-CD44 interaction further promoted HAS2 expression (control n = 17, HA n = 15). (**G**) HA-CD44 interaction increased CD44s isoform expression (control n = 22, HA n = 20). (**H**) Anti-CD44 mAb treatment *in vivo* decreased tumor HAS2 expression (n = 6 tumors each). (**I**) WB of increased PI3K-4EBP1-SOX2 pathway activation with CD44s OE. Vinculin and GAPDH served as loading controls. (**J**) Macrophage presence increased CD44s expression on cancer cells (alone n = 20, co-culture n = 20). (**K**) Macrophage presence increased cancer cell HAS2 expression (alone n = 20, co-culture n = 20). (**L**) Cancer cells in co-culture produced significantly higher HA. (**M**) Mechanistic overview of HAS2/HA/CD44 pathway promoting a feedback loop which promoted PI3K-4EBP1-SOX2 signaling. HA dose depicted = 50μg/mL. For HA ELISA data, two technical repeats were performed. Statistical significance in **B**, **C**, **D**, **E**, **F**, **G**, **I**, **J** and **K** determined by 2-tailed unpaired Student's *t* test *$P<0.05$, **$P<0.01$, ***$P<0.001$, ****$P<0.0001$. For **A** and **H**, scale bars: 100μm. For **B**, **D**, **F**, **G**, **J**, and **K**, scale bars: 50μm.
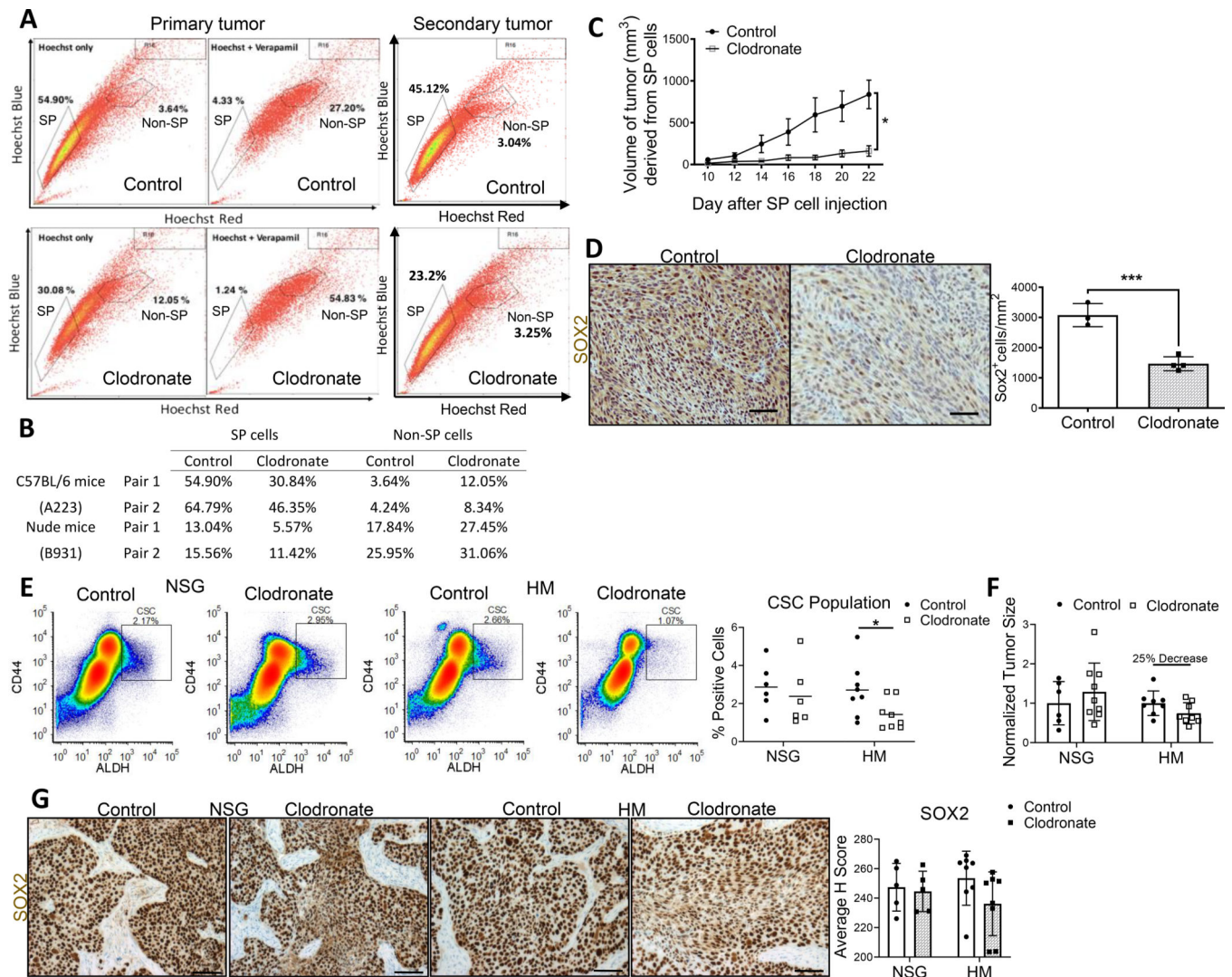
Figure 5. Macrophage depletion reduces CSC population, tumor size, and SOX2 *in vivo*.
(**A**) Representative flow diagrams for control and clodronate A223 treated tumors demonstrate decreased percentage of SP cells for primary and secondary tumors. Secondary tumors refer to SP cells isolated from primary tumors and transplanted into new recipient mice. (**B**) Reduced SP cell and Non-SP cell populations in clodronate treated mice. Two pairs analyzed per model group. (**C**) TAM depletion in mice decreased murine SCC tumor growth (mm^3). (**D**) Mouse SCC tumor SOX2 expression decreased with macrophage depletion. Left, representative tumor regions in control and clodronate treated tumors. Right, quantification of SOX2+ cells per mm^2 tumor for selected regions (control n = 3, clodronate n = 4). (**E**) Percent CSC population significantly reduced in HM clodronate treated tumors compared to control, but not in NSG clodronate treated tumors (NSG control n = 6, NSG clodronate n = 6, HM control n = 8, HM clodronate n = 8). (**F**) After 4 weeks clodronate treatment, HM treated tumors were 25% smaller than HM control tumors and 42% smaller than NSG treated tumors, negating null hypothesis (NSG control n = 6, NSG clodronate n = 9, HM control n = 8, HM clodronate n = 8). (**G**) Human HNSCC PDX SOX2 expression

was reduced in HM clodronate treated mice, but not in NSG clodronate treated mice (n = 5 for NSG groups, n = 8 for HM groups). N values represent number of tumors analyzed. For **D** and **G**, scale bars: 100μm. Statistical significance in **C**, **D**, and **E** determined by 2-tailed unpaired Student's *t* test *$P<0.05$, ***$P<0.001$.
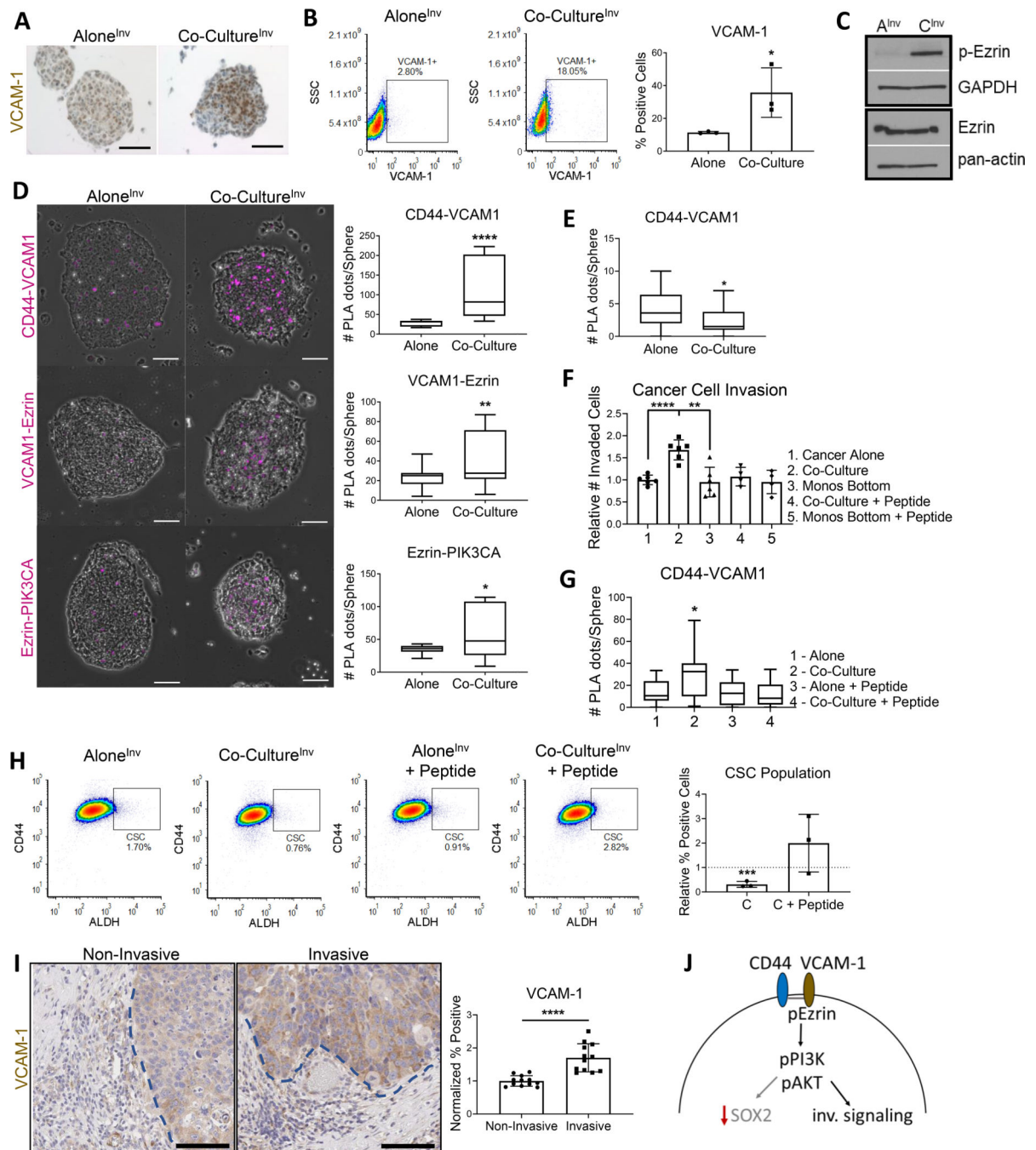
Figure 6. CD44-VCAM-1 drives monocyte influenced HNSCC cancer cell invasion.
For **D**, **E**, and **G**: Plot of one representative PLA repeat shown. All PLAs repeated 2–3
times, and n = # spheres quantified for each condition. (**A**) Co-culture^{Inv} spheres
demonstrated higher VCAM-1 expression via IHC. (**B**) Cancer cells co-cultured with
monocytes expressed higher surface VCAM-1 than cancer cells cultured alone; 3 separate
repeats shown. (**C**) WB of cancer cells co-cultured (C^{Inv}) or cultured alone (A^{Inv}). Co-
cultured cancer cells had higher activated (phosphorylated) Ezrin. GAPDH and pan-actin
used as loading controls. (**D**) PLAs of invasion spheres demonstrate increased CD44-

VCAM1 interaction, VCAM-1 recruitment of Ezrin, and Ezrin association with PIK3CA in co-culture conditions. Left, representative images of spheres containing magenta PLA dots. Right, quantification plots (n = 16–21 for all). (**E**) CD44-VCAM-1 interaction not abundant in co-culture[GP] model (n = 36 each). (**F**) VCAM-1 blockade eliminated invasion advantage provided by monocytes. Two wells plated per repeat, and 3 repeats performed. (**G**) VCAM-1 blockade of monocyte binding reduced CD44-VCAM1 interaction in co-culture spheres (n = 24 for all). (**H**) VCAM-1 blockade reversed co-culture invasive phenotype and promoted increased percent CSC population. Left, representative flow diagrams of one repeat. Right, quantification of 3 repeats normalized to respective controls (y = 1 for alone (co-culture control) and y = 1 for alone + peptide (co-culture + peptide control)). (**I**) Representative patient cases CUHN004, CUHN013, CUHN026 and CUHN043 were assessed for VCAM-1 expression at non-invasive and invasive tumor edges indicated by blue dotted lines, respectively. VCAM-1 was significantly higher at invasive edges. Scale bars: 100μm. (**J**) Mechanistic overview of CD44-VCAM1 interaction promoting recruitment and activation of Ezrin, which in turn activates (phosphorylates) PI3K and promotes invasive signaling. Statistical significance in **B**, **D**, **F**, **G**, **H** and **I** determined by 2-tailed unpaired Student's t test *P<0.05, **P<0.01, ***P<0.001, ****P<0.0001.
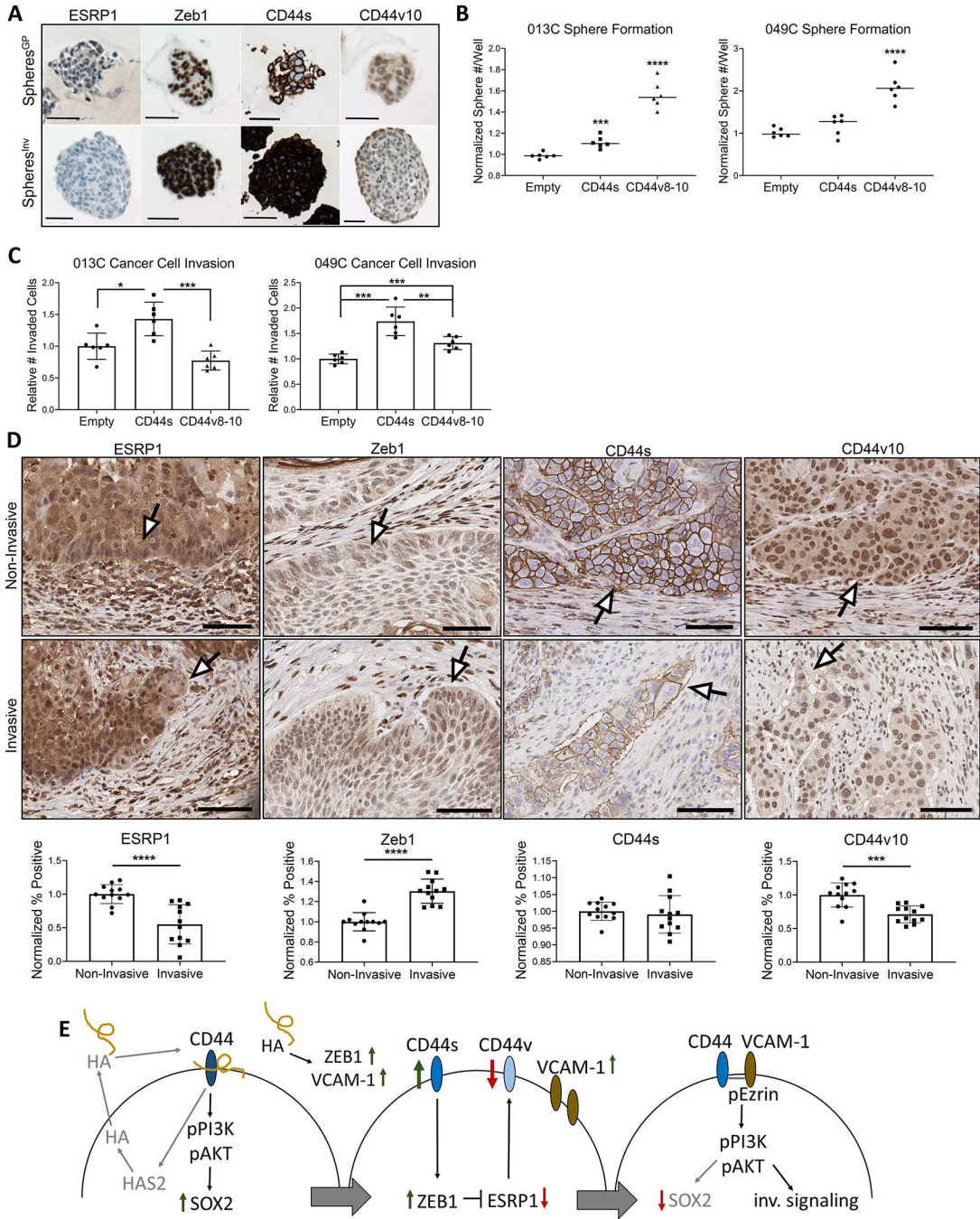
Figure 7. CD44 shift via Zeb1/ESRP1 feedback allows stemness-to-invasion switch.
(**A**) Representative IHC images of CD44 isoform and associated regulators Zeb1 and ESRP1 expression for spheroids of each model system. High ESRP1 and CD44v8-10 complex expression (measured by anti-CD44v10) represent a more epithelial phenotype. Low ESRP1, high Zeb1, and high CD44s expression represent a more mesenchymal phenotype. (**B**) CD44 isoform expression influences cancer cell sphere formation capability. CD44v8-10 expression promoted the greatest sphere formation. Three wells plated per repeat and 2 repeats performed. (**C**) CD44s expression promotes greater cancer cell invasion. Two wells

plated per repeat and 3 repeats performed. (**D**) Top: representative images (20x) of patient tissue depicting ESRP1, Zeb1, CD44s, and CD44v10 at non-invasive vs invasive edges. White arrows point to expression changes at respective edge. Bottom: quantification of ESRP1, Zeb1, CD44s, and CD44v10 expression at non-invasive and invasive edges supporting observed trend in representative patient cases CUHN004, CUHN013, CUHN026, and CUHN043. (**E**) Full mechanistic overview for proposed growth-to-invasion switch. Statistical significance in **B**, **C**, and **D** determined by 2-tailed unpaired Student's *t* test *$P<0.05$, ***$P<0.001$, ****$P<0.0001$. Scale bars:100μm.